Development of a Library of Adult Computational Phantoms Based on Anthropometric Indexes

Azadeh Akhavanallaf, Tianwu Xie, and Habib Zaidi, *Fellow, IEEE*

***Abstract*—Computational phantom libraries have been developed over the years to enhance the accuracy of Monte Carlo-based radiation dose calculations from radiological procedures. In this paper, we report on the development of an adult computational anthropomorphic phantom library covering different body morphometries among the 20–80 years old population. The anatomical diversities of different populations are modeled based on anthropometric parameters extracted from the National Health and Nutrition Examination Survey database, including standing height, total weight, and body mass index. Organ masses were modified to match the corresponding data. The ICRP reference male and female models were selected as anchor phantoms. A computer code was developed for adjusting standing height and percentage of fat free mass of anchor phantoms by 3-D scaling. The waist circumference and total body mass were further adjusted. The diversity of organ masses due to anthropometric differences deviates from the mean values by about 3%–21%, while this deviation exceeds 50% for genital organs. Thereafter, organ-level absorbed doses from both internal and external radiation exposure conditions were estimated. A total of 479 phantoms corresponding to seven age groups were constructed for both genders, thus fulfilling the criteria for representing a diverse adult population with different anthropomorphic and anatomical characteristics.**

***Index Terms*—Anthropometric data, computational phantoms, Monte Carlo (MC), radiation dosimetry, simulations.**

I. Introduction

THE utilization of radiation-based diagnostic imaging systems is progressively increasing worldwide, raising concerns about the potential hazards of radiation exposure. Computational phantoms were developed to accurately model radiation interaction within the human body using Monte Carlo (MC)-based radiation transport software packages targeting a number of applications, including radiation dose calculations and imaging physics research [1]. The first generation of computational phantoms were defined by simple surface equations and initially developed in the 1960s [2]. In the late 1980s, following the advent of tomographic medical imaging technologies, such as CT and MRI, voxel-based phantoms were developed to represent the anatomical features of the human body. Voxel-based phantoms were rapidly adopted in MC simulations owing to their ability to model anatomical details and have been continued to be developed over the years taking advantage from advances in high-resolution imaging. The third generation of computational phantoms using boundary representation techniques emerged in the form of nonuniform rational B-splines (NURBS) or polygon mesh surfaces. They offer better flexibility in terms of modeling deformation, motion, and change in posture [3]–[5].

From a radiation protection perspective, it is essential to determine and quantify the variability of radiation dose with respect to variations in anthropometry and anatomy. To this end, anthropomorphic phantoms coupled with MC methods play an important role in radiation dosimetry calculations. Reference anthropomorphic models were developed based on the average population [4], [6]–[8] but limited to fixed anthropometric and anatomical parameters. However, the diversity of anthropometric parameters between reference models and individuals may introduce significant uncertainties, thus motivating and raise the demand of personalized computational phantoms. Although, person-specific phantoms added up to an ideal model, some limitations such as lack of high-resolution tomographic images for each person and a time consuming segmentation process drew the attention of researchers to a more efficient approach of computational phantoms in medical dosimetry. Habitus-specific phantoms introduced as a size adjustable type of phantoms which were constructed based on deformation in a reference phantom. These phantoms are neither too individualized like subject-specific phantoms nor population-averaged as are reference phantoms [3], [9].

A number of studies focused on size-adjustable phantoms to account for variability in body size, organ masses, and other parameters, such as body fat percentage and subcutaneous fat distribution in dosimetry applications. Johnson *et al.* [9] built patient-dependent phantom series containing 25 models based on the University of Florida (UF) hybrid adult male phantom [8] using anthropometric parameters extracted

Manuscript received January 4, 2018; revised March 8, 2018; accepted March 12, 2018. Date of publication March 16, 2018; date of current version December 31, 2018. This work was supported in part by the Swiss National Science Foundation under Grant SNSF 320030_176052, in part by the Swiss Cancer Research Foundation under Grant KFS-3855-02-2016, and in part by the Iran's Ministry of Science and Technology. *(Azadeh Akhavanallaf and Tianwu Xie contributed equally to this work.) (Corresponding author: Habib Zaidi.)*

A. Akhavanallaf and T. Xie are with the Division of Nuclear Medicine and Molecular Imaging, Geneva University Hospital, CH-1211 Geneva, Switzerland (e-mail: azadeh.akhavanallaf@etu.unige.ch; tianwuxie@gmail.com).

H. Zaidi is with the Division of Nuclear Medicine and Molecular Imaging, Geneva University Hospital, CH-1211 Geneva, Switzerland, also with the Geneva Neuroscience Center, Geneva University, CH-1205 Geneva, Switzerland, also with the Department of Nuclear Medicine and Molecular Imaging, University of Groningen, University Medical Center Groningen, 9700 RB Groningen, The Netherlands, and also with the Department of Nuclear Medicine, University of Southern Denmark, 500 Odense, Denmark (e-mail: habib.zaidi@hcuge.ch).

Color versions of one or more of the figures in this paper are available online at http://ieeexplore.ieee.org.

Digital Object Identifier 10.1109/TRPMS.2018.2816072

from National Health and Nutrition Examination Survey (NHANES) III (1988–1994). The phantoms were remodeled considering two classes of target parameters: 1) primary parameters (body height and weight) and 2) secondary parameters (waist and thigh circumferences). The internal organ masses of Johnson's models deviated from reference values due to the 3-D scaling during the deformation process.

In another study, an automated algorithm was developed to generate an adult phantom library using polygon mesh surfaces where the Rensselaer Polytechnic Institute adult male and adult female models [4] were extended into a library representing morphometric diversities in the U.S. population for the 19-year old males and females. The organ masses were assumed to follow a Gaussian normal distribution [10] according to the mean and standard deviation compiled from various sources [5].

A study was performed by Broggio *et al.* [11] to construct a library of 25 adult males using NURBS surfaces constructed based on full body optical models. The anthropometric parameters were extracted from Civilian American and European Surface Anthropometry Resource with 109 identified organs scaled by ICRP reference data and height-dependent linear formula [12], [13]. Cassola *et al.* [14] produced a library of 18 phantoms from FASH and MASH mesh-based anchor phantoms using 3-D modeling software where the organ masses were scaled as a function of height [15].

The first library of 4-D phantoms comprising 58 NURBS models was developed by Segars *et al.* [16]. This library was extended based on reference XCAT phantoms [17] using real anatomy of chest-abdomen-pelvis CT data of normal patients having different body mass indices (BMIs). A library of 84 adult phantoms based on the Chinese Reference Adult Male polygon Surface (CRAM_S) was constructed by Chen *et al.* [18] where the organ models were adjusted to match reported Chinese reference data. An extended library of UF family containing 351 computational phantoms has also been developed based on morphometric data from NHANES (1999-2006) [19].

In the previous works, attention was paid to reflect more realistically the distribution of physical properties while the anatomical diversities were not appropriately considered. Different approaches have been adopted to determine organ masses representative of the considered population for the design of computational phantoms. For instance, organ masses can be set to reference values or deviate from reference masses during 3-D scaling. Alternatively, organ masses were linearly correlated to only phantom statures or simply sampled using a normal distribution. A practical approximation to realistically model the anatomical variability among individuals consists in implementing multiple correlations of each organ mass with different external anthropometric parameters into the phantom series.

In this paper, a software tool was developed to automatically remodel anchor reference phantoms to match target morphometric and anatomical characteristics. The developed library of voxel-based models is capable of representing internal details unlike surface models that cannot represent an inhomogeneous density distribution of organs or tissues [20]. The diversity of 13 organ masses depending on different morphometric parameters was considered. ICRP male and female voxel phantoms [21] were selected as reference models. A total of 230 male and 249 female adult voxel-based phantoms were constructed considering the diversity of anthropometric parameters from NHANES (2011-2014) [22] and variability in internal organ masses between individuals. As an application, MC-based dosimetry calculations using the developed phantom library were performed for internal and external radiation exposure conditions.

TABLE I
MAIN CHARACTERISTICS OF THE ICRP ADULT MALE AND FEMALE REFERENCE COMPUTATIONAL PHANTOMS

REFERENCE PHANTOM PROPERTIES	MALE	FEMALE
HEIGHT (cm)	176	163
MASS (Kg)	73.0	60.0
NUMBER OF TISSUE VOXELS	1,946,375	3,886,020
SLICE THICKNESS (VOXEL HEIGHT, mm)	8.0	4.84
VOXEL IN-PLANE RESOLUTION (mm)	2.137	1.775
VOXEL VOLUME (mm^3)	36.54	15.25
NUMBER OF COLUMNS	254	299
NUMBER OF ROWS	127	137
NUMBER OF SLICES	222	348

II. MATERIAL AND METHODS

A. ICRP Adult Reference Phantoms

The ICRP phantoms were constructed through modification of the voxel models (Golem and Laura) of a 38-year-old male (176 cm, 70 kg) and a 43-year-old female individual (167 cm, 59 kg), whose body height and mass resembled the physical characteristics of the reference male and reference female phantoms. In total, 140 organs with 53 tissue types were segmented and the organ masses of both models adjusted to the ICRP data of the adult reference male and female [21], [23]. The main characteristic of these phantoms are summarized in Table I.

B. Anthropometric Data

The field of anthropometry encompasses a variety of human body measurements, such as weight, height, circumferences, and lengths to represent the physical characteristics of a population. According to the trends of obesity among individuals, an updated database is required to represent a realistic body morphometry distribution. As shown in Fig. 1, the results of anthropometric reference data from 1999 to 2014 reflect the obesity prevalence in the U.S. population [24]. In the present study, morphometric parameters in seven age groups from 20 to 80 years old were obtained from the recently published NHANES (2011–2014) database. Height–weight grids obtained from the combination of height and weight percentile data (10%, 15%, 25%, 50%, 75%, 85%, and 90%) and BMI range, indicating the ratio of weight to squared height, were carefully selected to limit unrealistic physical properties.

C. Fat Free Mass and Waist Circumference Target Values

Since the extraction of a precise model for calculation of fat percentage and related fat free mass (FFM) percentage

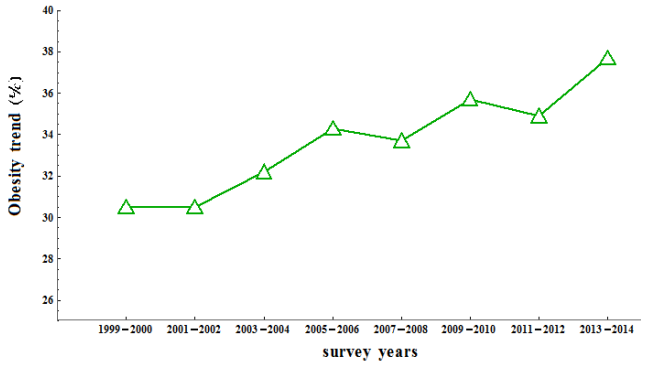

Fig. 1. Trends in obesity prevalence among adults aged 20 and over, United States, 1999–2000 through 2013–2014.

correlated with anthropometric parameters is not straightforward, the average values of different models reported in the literature were derived. The results show that FFM percent increases by increasing the height and decreases by increasing BMI [25]–[27]. Although both BMI and waist circumference measure the level of obesity, waist circumference may be more important because it is more sensitive to the distribution of body fat than BMI. To construct a more realistic body shape, waist circumference data extracted from NHANES (2011–2014) was combined with a linear model of waist circumference proportional with BMI using demographic data obtained from NHANES (2003) [28], [29].

D. Correlation Between Organ Masses and Anthropometric Parameters

One of the most important factors influencing radiation dosimetry calculations is the mass of organs, which substantially vary between different subjects owing to specific anatomical characteristics. In the absence of person-specific imaging data, the estimation of organ masses relies on their correlation with external physical parameters. To this end, organ mass data were extracted from anthropometric parameters including age, standing height, body weight, and BMI of an individual. A survey of published articles reporting organ masses in correlation with morphometric parameters is given in Table II. In this paper, 13 organ masses including brain, heart, right and left lungs, liver, spleen, thyroid, right and left kidneys, pancreas, and three genital organs for each gender were extracted from derived from autopsies and diagnostic measurements [12], [30]–[41]. Information on organ masses from different scientific publications has been culled in a software to extract the masses of 13 organs based on specific anthropometric parameters.

E. Methodology for Automated Model Deformation

In this paper, an automated algorithm was developed to remodel the reference phantom into various anthropometric and anatomical data. Computer software written in MATHEMATICA 7 (Wolfram Research Inc, Champaign, IL, USA) coupled with MATLAB 8.1 scripts (The MathWorks Inc., Natick, MA, USA) was used to implement the whole

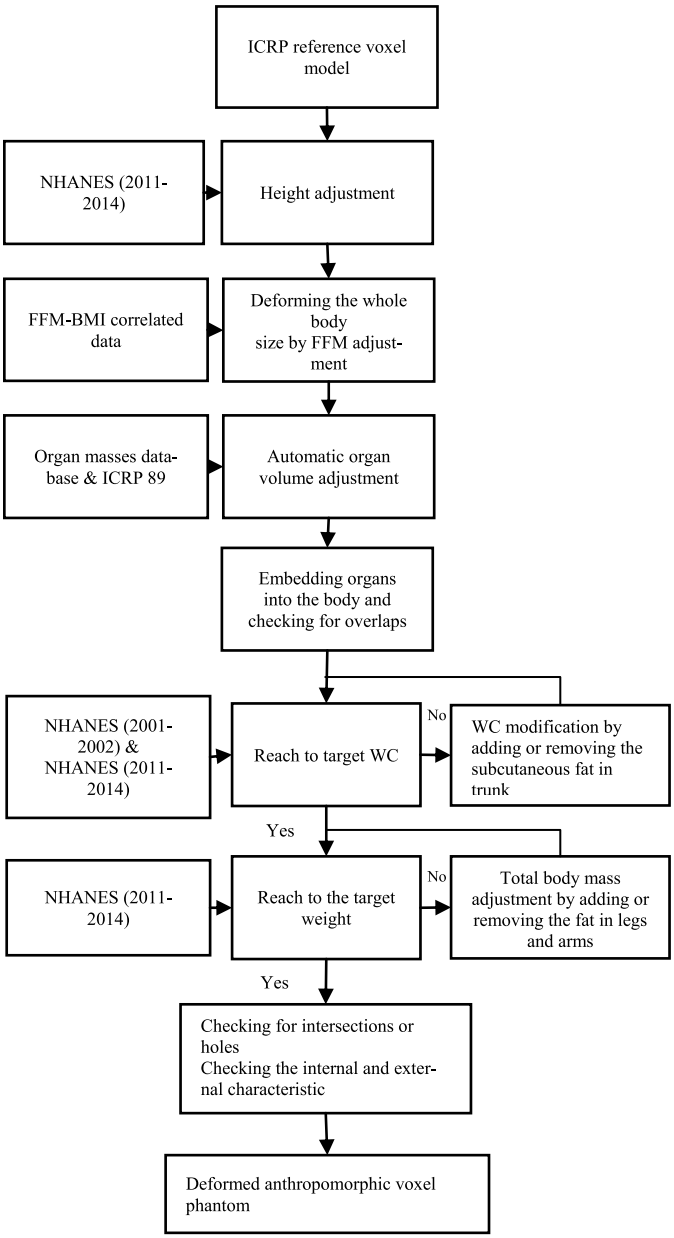

Fig. 2. Flowchart of the deformation process.

deformation process schematically displayed in Fig. 2. In the reference phantoms, the blood vessels were inwardly replaced in 2-D to avoid losing the vessels located in the residual tissue region during the adjustment of the fat mass for thin phantoms. The first step to reach the target anthropometric parameters consists in adjusting the height. Once the height is exactly matched, deforming the whole frame of phantoms using FFM percent was done by rescaling the phantom in 2-D. To adjust organ masses, the deformation process was applied on each organ to fine tune the volume, considering the conservation of organ's center of mass position. In addition to the 13 organs scaled in association with anthropometric parameters, four other organs including gall bladder, stomach, thymus, and urinary bladder were scaled to ICRP reference masses. The scaled organs were embedded into the body where the centroid position of each organ was kept constant through

TABLE II
SUMMARY OF THE MAIN PUBLICATIONS REPORTING ON ORGAN MASS ESTIMATION BASED ON CORRELATIONS WITH ANTHROPOMETRIC PARAMETERS

REFERENCE	STUDIED POPULATION	ORGANS /FAT FREE MASS/ FAT MASS /WAIST CIRCUMFERENCE	ANTHROPOMETRIC PARAMETERS				GENDER	STATISTICAL ANALYSIS	COMMENTS
			HEIGHT	WEIGHT	AGE	BMI			
MANDAL ET AL. [31]	300	BRAIN, HEART, LUNGS, LIVER, SPLEEN, THYROID, KIDNEYS, UTERUS/PROSTATE			✓	✓	M/F	LINEAR CORRELATION	HIGHER ORGAN MASSES IN HIGHER BMI (BOTH GENDERS) AND YOUNGER AGES (LIVER, SPLEEN, KIDNEY)
SHEIKHAZADI ET AL. [32]	1222	BRAIN, HEART, LUNGS, LIVER, SPLEEN, THYROID, KIDNEYS, PANCREAS, TESTIS, UTERUS/PROSTATE	✓		✓	✓	M/F	LINEAR CORRELATION	ORGAN MASSES INCREASE WITH BODY HEIGHT AND BMI VALUES
GRANDMAISON ET AL. [13]	684	HEART, LUNGS, LIVER, SPLEEN, THYROID, KIDNEYS, PANCREAS	✓		✓	✓	M/F	LINEAR CORRELATION	ORGAN MASSES DECREASE WITH AGE EXCEPT FOR HEART, THYROID AND PROSTATE
MOLINA & DIMAIO [34]	232	BRAIN, LUNGS, LIVER, SPLEEN, KIDNEYS				✓	M	STATISTICAL CATEGORIZATION	REFERENCE RANGE
MOLINA & DIMAIO [33]	102	BRAIN, LUNGS, LIVER, SPLEEN, KIDNEYS				✓	F	STATISTICAL CATEGORIZATION	REFERENCE RANGE
MOLINA & DIMAIO [36]	232	HEART	✓	✓		✓	M	STRONG LINEAR CORRELATION	REFERENCE RANGE/ HEART MASS INCREASES LINEARLY WITH INCREASE IN BODY WEIGHT
MOLINA & DIMAIO [35]	102	HEART	✓	✓		✓	F	STRONG LINEAR CORRELATION	
HE ET AL. [37]	111	BRAIN, LIVER, SPLEEN, KIDNEYS	✓	✓	✓		M/F	MULTI-CORRELATION FORMULA	MRI STUDY/ SMALLER ORGAN MASSES AT HIGHER AGES, EXCEPT HEART
HEYMSFIELD ET AL. [38]	411	BRAIN, LIVER	✓		✓		M/F	EXPONENTIAL APPROXIMATION	LIVER SCALED WITH HEIGHT (POWER≈2), MALE BRAIN (POWER≈0.83)
CHOUKER ET AL. [43]	728	LIVER		✓	✓	✓	M/F	MULTI-CORRELATION FORMULA	LIVER MASS INCREASES WITH WEIGHT, DECREASES WITH AGE OLDER THAN 50-60 Y
KELSEY ET AL. [44]	5999 4	OVARY			✓		F	STATISTICAL CATEGORIZATION / POLYNOMIAL	MRI STUDY/ 69% OF THE VARIATION IN OVARIAN VOLUME IS DUE TO AGE
PERVEN ET AL. [39]	140	OVARY			✓		F	STATISTICAL CATEGORIZATION	OVARIAN VOLUME SHRINKING WITH AGE IN ADULTS
KELSEY ET AL. [40]	1418	UTERUS			✓		F	STATISTICAL CATEGORIZATION/POLYNOMIAL	AGE: 0-40 Y/ 84% OF THE VARIATION IN UTERUS VOLUMES IS DUE TO AGE
XIA ET AL. [42]	1301	PROSTATE			✓		M	STATISTICAL CATEGORIZATION	PROSTATE VOLUME GROWTH WITH AGE
ZHANG ET AL. [41]	1000	PROSTATE			✓		M	POLYNOMIAL FORMULA	PROSTATE VOLUME GROWTH WITH AGE
HEYMSFIELD ET AL. [28]	1318 3	FFM	✓		✓		M/F	EXPONENTIAL APPROXIMATION	FFM SCALE TO HEIGHT WITH POWER ~2
MEEUWSEN ET AL. [26]	2362 7	FM				✓	M/F	CURVILINEAR RELATIONSHIP	FM PERCENT ROSE COMPARED TO AN INCREASE IN BMI
SCHUTZ ET AL. [27]	5635	FM, FFM				✓	M/F	CURVILINEAR RELATIONSHIP	
BOZEMAN ET AL. [30]		WC				✓	M/F	LINEAR CORRELATION	NHANES (2003)

M (MALE), F (FEMALE), FFM (FAT FREE MASS), FM (FAT MASS), WC (WAIST CIRCUMFERENCE)

the phantom. To avoid the overlap of adjacent organs, a priority was defined for organs to be embedded according to their volume as well as their sensitivity to radiation. In the next step, for adjusting total body mass, first the waist circumference was considered as the estimation of belly fat. To this end, the outer contour of the phantom was detected, then adding or removing fat layer of the trunk was iterated until waist circumference was achieved. Waist circumference was measured at the uppermost lateral border of the hip crest (ilium) by measuring the perimeter of the outer body contour. Second, by tuning fat mass in the legs and arms, the target total body mass excluding the skin mass was fixed to within 3% of reference values. Lastly, the whole body phantom was checked for some intersections or holes and smoothness of outer contour, and the skin layer with a thickness equal to in-plain resolution was coated. After completion of the deformation process, each deformed phantom was visually analyzed in 2-D and 3-D to check the anatomical structures as well as whole body habitus.

F. Monte Carlo Calculations-Based Organ Dose Assessment

1) Internal Dose Estimation: The absorbed doses to three morphometrically different computational phantoms from ^{18}F-FDG as PET tracer were estimated through MC simulations using the N-particle extended (MCNPX) code. ^{18}F positron-emitting source with an average energy of 0.2498 MeV was simulated in six source regions according to ^{18}F-FDG biokinetic data reported in ICRP 106 [44]. A total number of 10^7 primary particles were generated to reach less than 1% statistical uncertainty in most cases [45], [46].

In the MIRD formalism, the radiation absorbed dose from any source organ r_S delivered to target tissue r_T is given by (1) [47]

$$D(r_T, T_D) = \sum_{r_s} \int_0^{T_D} A(r_s, t) S(r_T \leftarrow r_s) dt = \sum_{r_s} \tilde{A}(r_s, t) S(r_T \leftarrow r_s) \quad (1)$$

TABLE III
MORPHOMETRIC CHARACTERISTICS OF THE PATIENT AND FEMALE$_{40y\text{-}25h\text{-}75w}$ PHANTOM (40–50 YEARS AGE GROUP, 25TH PERCENTILE HEIGHT AND 75TH PERCENTILE WEIGHT)

CHARACTERISTICS	PATIENT	FEMALE$_{40y\text{-}25h\text{-}75w}$
SEX	FEMALE	FEMALE
AGE	50 y	40 -50 y
WEIGHT	88 Kg	85.3 Kg
HEIGHT	160 cm	158.1 cm
BMI	34.37	34.12

where $\tilde{A}(r_s, t)$ is the time integrated activity in the source organ during the dose-integration period T_D, $S(r_T \leftarrow r_s)$ is the S-value defining the equivalent dose rate in the target organ per unit activity in the source organ. Using MCNPX tally card ∗F8, S-values were estimated per particle. Time-integrated activity in the source organs were obtained from ICRP 106 [44] and the administered activity of ^{18}F-FDG was similar to PET/CT acquisition protocols used in our department (3.5 MBq/kg with a maximum of 350 MBq for patients heavier than 100 kg). The effective dose was calculated based on ICRP definition:

$$E = \sum W_T \sum W_R D_{T,R} \tag{2}$$

where E denotes the effective dose, W_R is the radiation weighting factor, $D_{T,R}$ is the absorbed dose in tissue or organ T, and W_T is the tissue weighting factor.

2) External Dose Estimation: To benchmark the CT radiation dose calculation using the developed library, the dose report of a female patient with high BMI who underwent a CT examination in our department under an IRB approved protocol was selected for comparison of the results with the corresponding phantom in the developed series. The characteristics of the patient and phantom are tabulated in Table III.

Examination details were extracted from the DICOM header. The study was performed on the Discovery CT 750 HD scanner (GE Healthcare, Waukesha, WI, USA) with a scan range covering the thorax and abdomen using the following acquisition parameters: a table speed of 55 mm/rot, 0.7 s revolution time, 1.37 pitch factor, and 40 mm total collimation width. A tube voltage of 120 kVp with tube current modulation (varying between 296 and 495 mA) were applied. CT dose was obtained using Radimetrics Enterprise Platform, a dose monitoring software tool using MC simulations (Bayer HealthCare) [48]. Radimetrics calculates patient-specific absorbed dose by adjusting the CT images of a patient with Cristy & Eckerman stylized computational phantom [49] considering sex, age, and size of body (diameter). To estimate the effective dose and absorbed dose in target organs of Female$_{40y\text{-}25h\text{-}75w}$, the CT acquisition parameters, a model of the 750 HD CT scanner and exposed phantom geometry were used as input to MCNPX [50], [51].

III. RESULTS

A. Anthropomorphic Parameters

The percentile data including 10%, 15%, 25%, 50%, 75%, 85%, and 90% of height and weight, extracted from the recent version of NHANES (2011–2014) database, were combined to provide 49 height–weight grids for each age group. To restrict unrealistic body morphometries, BMI percentile data varying from 19.8 to 40.7 kg/m^2 for adult females and from 20.5 to 36.9 kg/m^2 for adult males was assigned to the height–weight bins. Once BMI data were applied on grids, a total of 249 grids for females and 230 grids for males felt within acceptable BMI range. Figs. 3 and 4 display the height–weight grids of this library in seven age groups for females and males, respectively. Different categories of weight status include underweight individuals with BMI below 18.5, healthy people with BMI within the range 18.5–24.9, overweight, obese, and morbidly obese within BMI ranges 25.0–29.9, 29.9–39.9 and exceeding 40.0, respectively [19]. By combining weights and heights in this library, 33.7% of female models fall into the normal BMI category, 23.2% in overweight, 40.9% in obese, and 2% in morbidly obese. For male models, 27.8% of phantoms fall in healthy BMI class, 34.3% in overweight, and 37.8% in obese category.

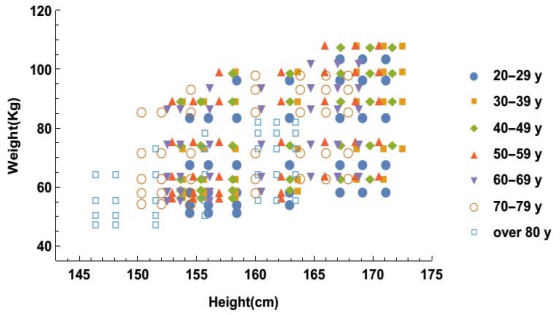

Fig. 3. Targeted grid for female phantoms in seven age groups.

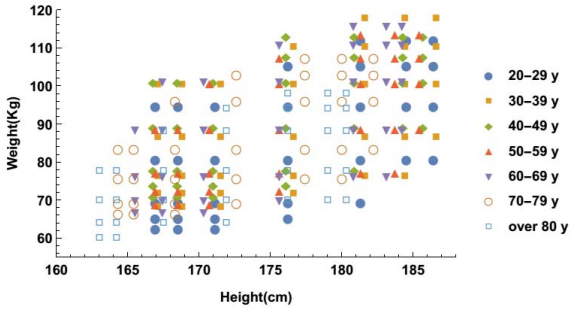

Fig. 4. Targeted grid for male phantoms in seven age groups.

The FFM percent and waist circumference were considered in this library as secondary parameters. The BMI and waist circumference parameters are widely used in the characterization of obesity. As depicted in Fig. 5, waist circumference increases with increasing BMI values, while the FFM is inversely proportional to BMI.

The diversity of organ masses as a function of four morphometric variables is illustrated in Table IV. These data are sampled based on anthropometric parameters of the phantoms belonging to the current library. The mean values of organ masses calculated by multiple correlation considering anthropometric variables show a deviation from ICRP reference organ masses, but still in the same order of magnitude.

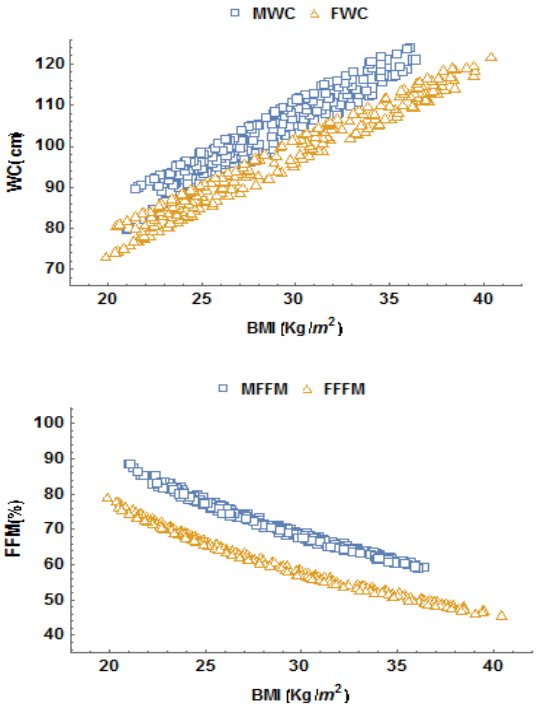

Fig. 5. Plots of waist circumference (top) versus BMI for males (MWC) and females (FWC) and FFM percent (bottom) versus BMI for males (MFFM) and females (FFFM).

TABLE IV
ORGAN MASSES CORRELATED WITH ANTHROPOMETRIC PARAMETERS FOR FEMALE AND MALE PHANTOMS

ORGANS	FEMALE ORGAN MASS (g)			MALE ORGAN MASS (g)		
	MEAN ± SD	ICRP	RANGE	MEAN ± SD	ICRP	RANGE
BRAIN	1226.9±20.64	1300	1184.46-1265.37	1380.9±20.57	1450	1336.53-1419.57
LUNG	491.83±9.2	475	471.32-502.27	621.24±17.17	600	587.15-649.48
KIDNEY	126.85±2.2	137	122.4-129.46	159.31±6.57	160	143.63-174.73
SPLEEN	149.52±12.13	130	127.32-180.99	197.01±22.04	150	153.60-250.99
PANCREAS	99.672±3.618	120	92.87-105.97	123.73±3.59	140	114.87-127.55
LIVER	1406.1±90.04	1400	1201.13-1601.02	1719.2±112.8	1800	1448.91-1942.58
HEART	595.95±9.618	620	571.42-605.24	879.71±14.80	840	847.05-902.42
THYROID	17.455±0.8127	17	16.24-18.54	23.911±0.72	20	22.16-25.3
OVARY	3.64±1.988	5.5	1.872-6.76	-	-	-
UTERUS	69.11±5.787	80	61.54-79.16	-	-	-
TESTES	-	-	-	21.312±0.177	17.5	20.96-21.51
PROSTATE	-	-	-	32.289±7.33	17	21.50-42.15

The difference between calculated organ masses and ICRP reference data falls within the range 0.4%–51%.

B. Deformed Phantoms

To demonstrate the variability of the morphometry of the developed phantoms, frontal, and rotated views of the ICRP female reference model compared with two female phantoms at 30–40 years age group at 10th percentile standing height and 75th percentile of body weight ($\text{Female}_{\text{30y-10h-75w}}$) and 90th percentile of standing height, and 50th percentile of body weight ($\text{Female}_{\text{30y-90h-50w}}$) are depicted in Fig. 6. The male ICRP reference model is compared in Fig. 7 to two male phantoms at 20–30 years age group, at 10th percentile standing height and 75th percentile of body weight ($\text{Male}_{\text{20y-10h-75w}}$) and 90th percentile of standing height, and 50th percentile of body weight ($\text{Male}_{\text{20y-90h-50w}}$).

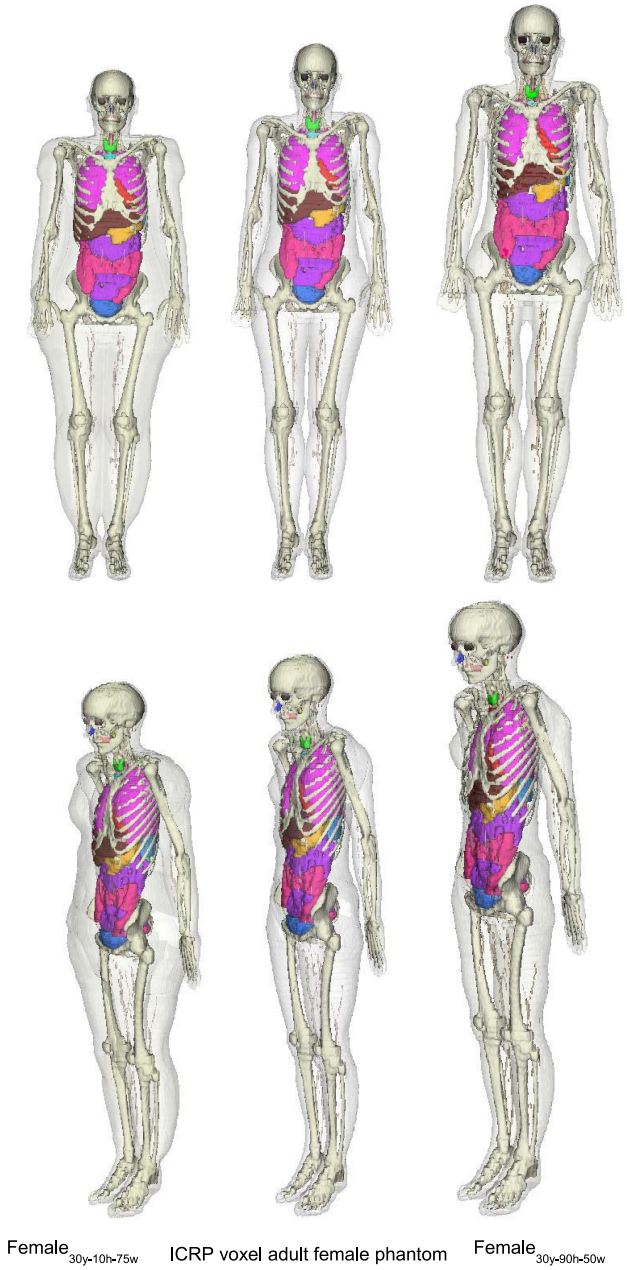

Fig. 6. Frontal and rotated views of the adult female phantoms at 30–40 year age group at 10th percentile standing height and 75th percentile of weight ($\text{Female}_{\text{30y-10h-75w}}$), ICRP voxel adult female phantom, 90th percentile of height and 50th percentile of weight ($\text{Female}_{\text{30y-90h-50w}}$).

We considered the diversity of internal organ masses between individuals to go one step closer to person-specific phantoms as standard models.

In this paper, an initial database of 13 internal organ masses was culled using the surveyed dependence of organ masses and anthropometric parameters shown in Table II. In Fig. 8,

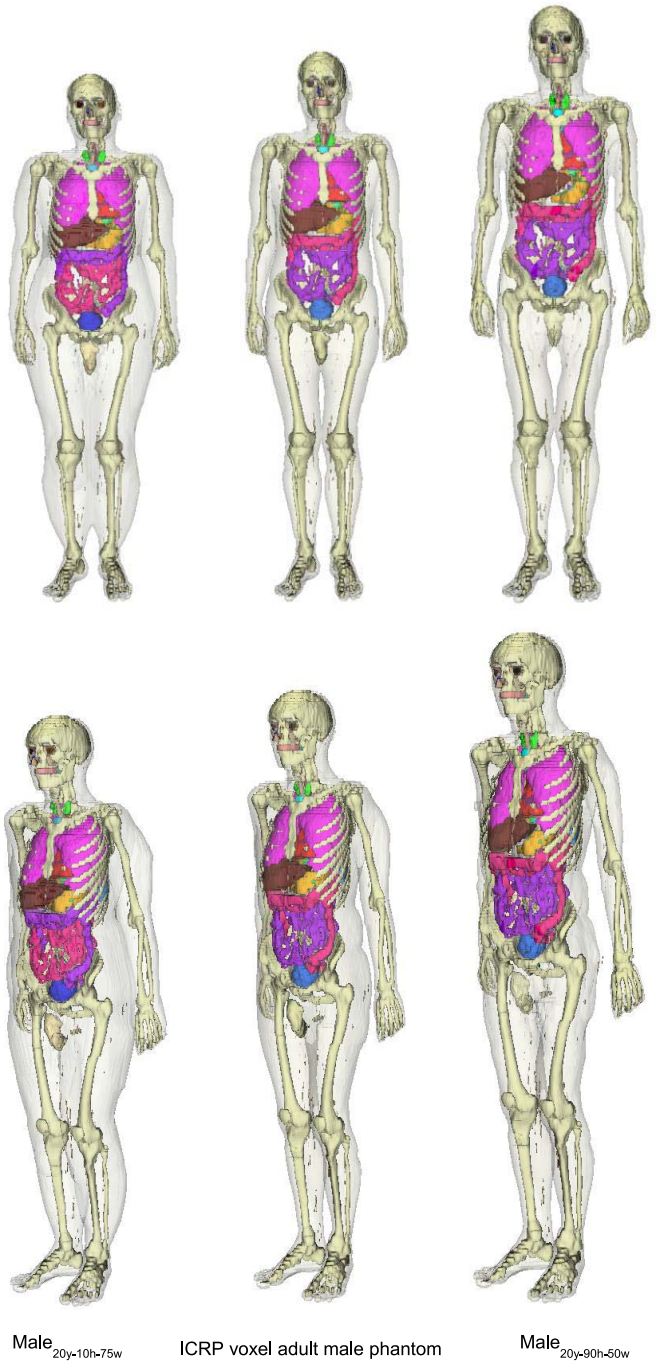

Fig. 7. Frontal and rotated views of adult male phantoms at 20-30 year age groups, at 10th percentile standing height and 75th percentile of weight ($Male_{20y\text{-}10h\text{-}75w}$), ICRP voxel male phantom, 90th percentile of height and 50th percentile of weight ($Male_{20y\text{-}90h\text{-}50w}$).

transaxial slices of two morphometrically different female phantoms with the same height but at different age groups and weight displaying obvious differences for the liver are shown.

The total body masses of the developed series were adjusted to target percentile values within 2% and waist circumference within 3% of target values. Evaluation of phantom anatomies was performed by scaling 17 organ masses correlated with morphometric parameters to agree within ±5% of target values. However, some cases have shown a larger deviation from

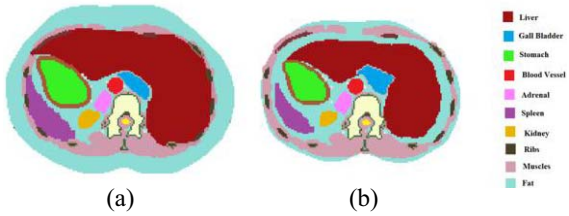

Fig. 8. Transaxial views of female phantoms displaying liver volume differences showing (a) 85th percentile of height and weight at age group 20–30 years and (b) 85th percentile of height and 25th percentile of weight at age group 60–70 years.

the target data because of interpolation errors for small organs and the overlap correction of adjacent organs. The deformation process was implemented on a PC with Intel Xeon Processor of 2.4 GHz. The computational time required for deforming the internal organs of the phantom is less than 2 min. Adjusting all of the anthropometric parameters takes in average about 20 min depending on the amount of fat mass requiring amendment.

C. Monte Carlo-Based Dosimetry Calculations

1) Internal Dose From ^{18}F-FDG: Absorbed dose to organs was calculated for three anthropomorphically different phantoms in both genders including female phantoms at age group 30–40 years representing $Female_{30y\text{-}10h\text{-}10w}$ (10th height and weight percentiles) and $Female_{30y\text{-}90h\text{-}90w}$ (90th height and weight percentiles) as well as ICRP female reference phantom They were also calculated for male phantoms in age group 30–40 years $Male_{30y\text{-}10h\text{-}15w}$ (10th height and 15th weight percentiles) at age group 50–60 years $Male_{50y\text{-}75h\text{-}50w}$ (75th height and 50th weight percentiles) in addition to ICRP male reference phantom. The simulation was designed for a whole body ^{18}F-FDG PET/CT protocol. Absorbed doses to six phantoms with different sex, age, and anthropometric parameters are reported in Table V. The absorbed dose per unit administered activity for the ICRP female reference phantom is about 35% higher than that of the obese female phantom ($Female_{30y\text{-}90h\text{-}90w}$). It is about 8.34% less in comparison with the thin phantom ($Female_{30y\text{-}10h\text{-}10w}$). The absorbed dose per unit administered activity for the ICRP male reference phantom is about 14.5% higher than the male obese phantom ($Male_{50y\text{-}75h\text{-}50w}$). It is about 1.5% less than that of the thin phantom ($Male_{30y\text{-}10h\text{-}15w}$). The total absorbed dose increases by increasing the body weights since the injected activity is proportional to patient weights (Table V).

The effective doses and absorbed doses per unit administered activity in target organs for female and male phantoms are illustrated in Figs. 9 and 10, respectively. The five organs receiving the highest absorbed doses in the simulated phantoms are the heart, bladder, brain, liver, and prostate for the male (uterus for female) phantom. The differences of absorbed doses in target organs between the ICRP female reference phantom and the habitus-dependent phantoms vary from −39% to 55.8%. They range between −37% and 28.7% for the male ICRP reference phantom. The differences of organ absorbed dose among phantoms depends on differences

TABLE V
SUMMARY OF ^{18}F-FDG ABSORBED DOSES FOR FEMALE PHANTOM AT SECOND AGE GROUP AND 10TH–10TH HEIGHT AND WEIGHT PERCENTILES, RESPECTIVELY ($\text{FEMALE}_{30y\text{-}10h\text{-}10w}$), ICRP REFERENCE FEMALE PHANTOM ICRPFEMALE, AND FEMALE PHANTOM AT SECOND AGE GROUP AND 90TH–90TH HEIGHT AND WEIGHT PERCENTILES, RESPECTIVELY ($\text{FEMALE}_{30y\text{-}90h\text{-}90w}$). SAME AS ABOVE FOR THE MALE PHANTOM AT SECOND AGE GROUP AND 10TH–15TH HEIGHT AND WEIGHT PERCENTILES, RESPECTIVELY ($\text{MALE}_{30y\text{-}10h\text{-}15w}$), ICRP REFERENCE MALE PHANTOM ICRPMALE, AND MALE PHANTOM AT FOURTH AGE GROUP AND 75TH–50TH HEIGHT AND WEIGHT PERCENTILES, RESPECTIVELY ($\text{MALE}_{50y\text{-}75h\text{-}50w}$). THE DIFFERENCES BETWEEN THE ICRP REFERENCE PHANTOM AND OTHER PHANTOMS ARE ALSO SHOWN

PHANTOM ID	WEIGHT (kg)	HEIGHT (cm)	BMI (kg/m^2)	ABSORBED DOSE PER UNIT ADMINISTERED ACTIVITY		ABSORBED DOSE FOR OUR PROTOCOL (mGy)
				(mGy/MBq)	DIFFERENCE (%)	
$\text{FEMALE}_{30y\text{-}10h\text{-}10w}$	54.75	153.8	23.145	1.51E-02	+8.34	2.89
$\text{ICRP}_{\text{FEMALE}}$	60	163.0	22.58	1.39E-02	-	2.92
$\text{FEMALE}_{30y\text{-}90h\text{-}90w}$	106.3	172.5	35.93	9.04E-03	-35.0	3.16
$\text{MALE}_{30y\text{-}10h\text{-}15w}$	72.2	167.1	25.88	1.20E-02	+1.5	3.04
$\text{ICRP}_{\text{MALE}}$	73	176.0	23.63	1.18E-02	-	3.02
$\text{MALE}_{50y\text{-}75h\text{-}50w}$	89.2	181.3	27.23	1.01E-02	-14.5	3.16

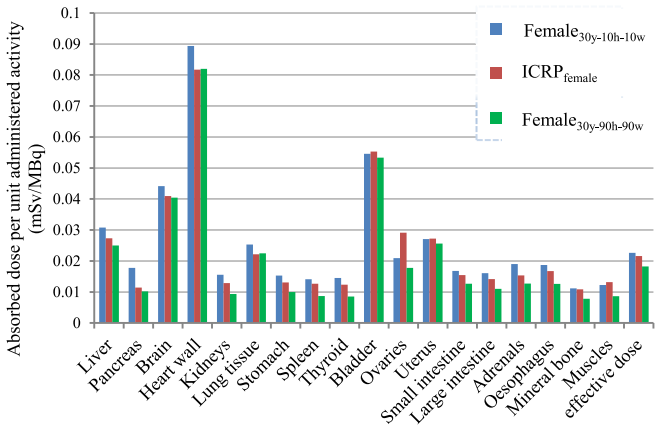

Fig. 9. Effective doses and absorbed doses per unit administered activity (mSv/MBq) in target organs for female phantoms at second age group and 10th–10th height and weight percentiles, respectively ($\text{Female}_{30y\text{-}10h\text{-}10w}$), 90th–90th height and weight percentiles, respectively ($\text{Female}_{30y\text{-}90h\text{-}90w}$) and the ICRP reference female phantom ($\text{ICRP}_{\text{female}}$).

in body structures and organ masses due to the different sex, age, and anthropomorphic characteristics. From the radiation protection standpoint, the effective dose as a single metric provides a practical information to compare different radiation exposure scenarios. The effective dose differences (in mSv/MBq) between ICRP female reference model and $\text{Female}_{30y\text{-}90h\text{-}90w}$ is about -15.6% and about 4.8% with $\text{Female}_{30y\text{-}10h\text{-}10w}$. For the ICRP male reference phantom, this difference is about -3.2% for $\text{Male}_{50y\text{-}75h-50w}$ and 7.6% with $\text{Male}_{30y\text{-}10h\text{-}15w}$.

2) External Dose From CT Examination: The absorbed dose in target organs of the patient extracted from Radimetrics package were compared with the results of morphometrically corresponding phantom $\text{Female}_{40y\text{-}25h\text{-}75w}$ (female phantom in

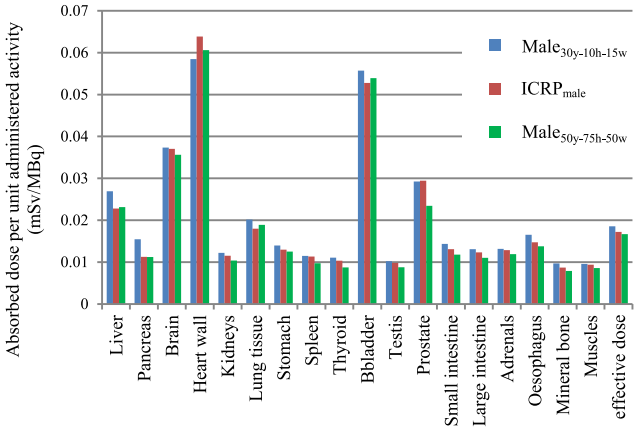

Fig. 10. Effective doses and absorbed doses per unit administered activity (mSv/MBq) in target organs for the male phantoms at second age group and 10th–15th height and weight percentiles, respectively ($\text{Male}_{30y\text{-}10h\text{-}15w}$), forth age group and 75th–50th height and weight percentiles, respectively ($\text{Male}_{50y\text{-}75h-50w}$) and the ICRP reference male phantom ($\text{ICRP}_{\text{male}}$).

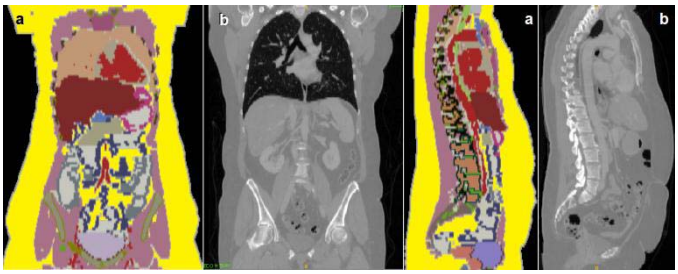

Fig. 11. Coronal (left) and sagittal (right) slices of (a) $\text{Female}_{40y\text{-}25h\text{-}75w}$ and (b) patient CT images.

age group 40–50 years, 25th percentile of height and 75th percentile of weight) under the same CT scanning conditions. Coronal and sagittal slices of patient CT images and $\text{Female}_{40y\text{-}25h\text{-}75w}$ phantom are shown in Fig. 11.

The comparison of absorbed doses for eight important organs and effective doses estimated by Radimetrics and our MC calculations is illustrated in Fig. 12. In most organs, the absorbed doses estimated by Radimetrics agree well with simulated results of $\text{Female}_{40y\text{-}25h\text{-}75w}$ with an average bias of about 16.6% (range 1.35%–43%). The lungs present the largest deviation (about 43%). Radimetrics reported an effective dose of 17.51 mSv whereas our simulations using $\text{Female}_{40y\text{-}25h\text{-}75w}$ resulted in an effective dose of 14.35 mSv.

IV. DISCUSSION

The construction of more realistic models representative of the adult population is highly desired for MC-based simulation studies targeting a number of research applications in diagnostic and therapeutic radiology. A new series of anthropomorphic phantoms extended from the ICRP reference phantoms covering not only the diversity of anthropometric characteristics but also anatomical diversities are developed in this paper. First, standing height and total body mass were adjusted as the primary parameters of this library. Second, FFM percent was tuned by 2-D scaling to make a more realistic proportion with anthropometric parameters between unscaled organs,

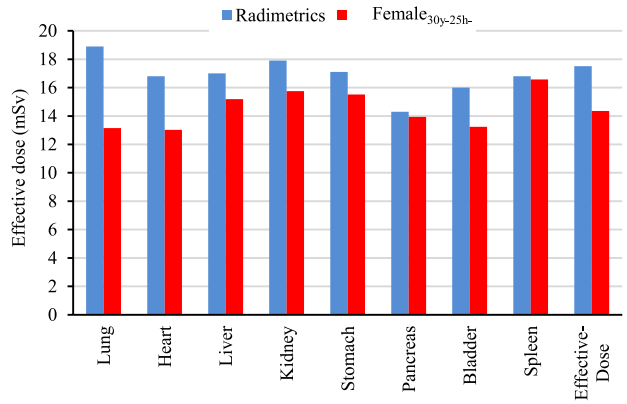

Fig. 12. Comparison of organ absorbed doses and effective doses between Radimetrics and MC simulations using $\text{Female}_{40\text{y-}25\text{h-}75\text{w}}$ phantom.

such as muscles and bones. Although different body shapes are not defined in this paper, tuning the FFM percent helps to appropriately change the body style of phantoms. In a few cases, such as 10th percentile of weight in the first age group of male phantoms, FFM percent was not applied on the reference phantom to reach the target waist circumference. By sampling from derived multiple correlations between organ masses and external anthropometric parameters (age, standing height, body weight, and BMI), organ mass data does not follow a normal distribution. According to the organ mass values in the library, the brain mass increases with increasing height and decreases with increasing age. For the lung, kidney, spleen, and pancreas, it can be concluded that their masses increase by increasing the body weight and BMI without following a meaningful correlation with height and age variations. The liver and heart masses are strongly proportional to the total body mass and consequently to BMI. The behavior of the thyroid is a little different since it first increases and then decreases with increasing standing height. Moreover, it has a smooth increase with age and weight. As mentioned earlier, genital organs strongly depend on the age, except testis mass which increases with weight and BMI. The mass of the ovaries decreases sharply after 35 years whereas the uterus mass reaches a peak at about 45 years and decreases at higher ages. The prostate mass increases strongly with age. The masses of remaining organs, such as the muscles, bones, blood vessels, ...etc. change after 3-D scaling as reported by Johnson *et al.* [9]. The masses of most organs deviate from the mean value by about 3%–21% while it exceeds 50% for genital organs.

The internal radiation dose was estimated in the context of a whole-body ^{18}F-FDG PET protocol for morphometrically different phantoms for both genders. The calculated absorbed doses per administered activity in target organs are in agreement with those reported by the ICRP 106 [44]. The effective dose for habitus-dependent phantoms varies between 1.82 and 2.26 (mSv/100 MBq) for females, and between 1.67 and 1.85 (mSv/100 MBq) for males, while the ICRP 106 reports an effective dose of 2.31 (mSv/100 MBq). As expected, a significant dose from ^{18}F-FDG is delivered to the heart, bladder, brain, liver, prostate for male and uterus for female. The heart, brain, and liver receive a considerable dose because of their high metabolic rate and hence rapid blood supply. The accumulation of radioactive urine in the bladder not only causes a significant self-absorbed dose but also leads to a high cross-organ dose to the uterus and prostate. Overall, thin patients receive a higher internal radiation dose because the cross-irradiation between internal organs is stronger than other patients. This can be justified by the lack of subcutaneous and visceral fat which directly influences cross-organ doses.

The organ-level doses and effective dose for the CT examination calculated for the anthropomorphic fitted phantom from the developed series show acceptable dose estimation accuracy for radiation protection purposes. Since each subject has exclusive anatomical characteristics, using an independent phantom library instead of a patient-specific model may cause a deviation from the actual absorbed dose. However, it definitely provides a more accurate estimate compared to the calculations using stylized phantoms, such as the Cristy & Eckerman stylized computational phantoms [49] implemented within Radimetrics software. During the course of this paper, we created a patient-specific model by segmenting a clinical CT study and compared the dose delivered to the patient-specific model, considered as reference, to results generated using the corresponding anthropomorphic phantom from our library and Radimetrics. The effective dose for the patient-specific model was estimated to be 11.72 mSv. The discrepancy between the effective dose calculated using the patient-specific model and the best fitting model from our library was 22.2%, whereas it was up to 49.2% when calculated using Radimetrics. As reported by Xie *et al.* [51], in addition to the anthropometric parameters, the organ-surface distance (average distance from the skin to organs) or body size shows a significant correlation with organ absorbed dose. It appears that Radimetrics overestimates the absorbed dose in target organs, particularly for the lungs.

In this paper, the diversity of organ masses is considered. However, for reliable modeling, a broad database is required to derive organ masses correlated with anthropomorphic variables. In addition, defining different somatotypes for the phantoms library makes it more comprehensive. Sheldon *et al.* [52] introduced three types of main somatotypes: 1) mesomorphs who are athletically built with a low percent of body fat; 2) ectomorphs who are underweight with a narrow skeleton frame; and 3) endomorphs who are overweight with a pear-shaped body style. In this paper, we set the FFM percent for different BMIs to consider body style in addition to the height and weight. By considering different styles in the future studies, the distribution of fat percent through the body of phantoms would be more realistic. Although the volume of intra-abdominal adipose tissue encompassed the organs is an important factor in the calculation of cross-organ dose, adjustment of this type of fat percent called visceral fat was ignored due to the lack of information, and total body mass was set by adjusting the subcutaneous fat mass.

Recent advances in deep learning are promoting a number of applications in computer vision and medical image analysis research that could be useful for constructing patient-specific models through automatic segmentation of body contours

and internal organs. Considering the scarcity of large clinical databases and time-consuming classification techniques required for organs labeling, generative networks can be used for developing data-hungry deep learning algorithms. Novel unsupervised models, such as variational auto-encoders [53] or generative adversarial networks [54] have shown potential in medical image analysis and look promising for applications involving the generation of synthesized medical images to fulfill the requirement of large training datasets, e.g., auto-segmentation [55].

V. Conclusion

An algorithm was developed to consider the diversity of organ masses along with the morphometric parameters to construct a library by automatic remodeling the voxel-based ICRP adult reference phantoms. Data on 13 organ masses is culled based on information from autopsies and diagnostic examinations. Using the specific anthropometric data of each individual, it is possible to derive organ masses data and automatically construct habitus-specific phantoms according to the specific input parameters.

By using habitus-dependent anthropomorphic libraries, the calculation of absorbed doses for individuals exposed to external or internal radiation is likely to be more accurate by considering the anthropomorphic and anatomical diversity among the population. The move toward subject-specific phantoms is a major improvement taking advantage of the availability of habitus-dependent phantoms associated with morphometric parameters and classified in different somatotypes.

References

[1] H. Zaidi, "Relevance of accurate Monte Carlo modeling in nuclear medical imaging," *Med. Phys.*, vol. 26, no. 4, pp. 574–608, 1999.

[2] H. Zaidi and X. G. Xu, "Computational anthropomorphic models of the human anatomy: The path to realistic Monte Carlo modeling in medical imaging," *Annu. Rev. Biomed. Eng.*, vol. 9, no. 1, pp. 471–500, 2007.

[3] X. G. Xu, "An exponential growth of computational phantom research in radiation protection, imaging, and radiotherapy: A review of the fifty-year history," *Phys. Med. Biol.*, vol. 59, no. 18, pp. R233–R302, Sep. 2014.

[4] J. Zhang, Y. H. Na, P. F. Caracappa, and X. G. Xu, "RPI-AM and RPI-AF, a pair of mesh-based, size-adjustable adult male and female computational phantoms using ICRP-89 parameters and their calculations for organ doses from monoenergetic photon beams," *Phys. Med. Biol.*, vol. 54, no. 19, pp. 5885–5908, 2009.

[5] Y. H. Na, B. Zhang, J. Zhang, P. F. Caracappa, and X. G. Xu, "Deformable adult human phantoms for radiation protection dosimetry: Anthropometric data representing size distributions of adult worker populations and software algorithms," *Phys. Med. Biol.*, vol. 55, no. 13, pp. 3789–3811, 2010.

[6] ICRP, *Report of the Task Group on Reference Man*. New York, NY, USA: Pergamon Press, 1975.

[7] M. Cristy, "Mathematical phantoms representing children of various ages for use in estimates of internal dose," Oak Ridge Nat. Lab., Oak Ridge, TN, USA, Rep. TNORNL/NUREG/TM-367, 1980.

[8] C. Lee, D. Lodwick, J. L. Williams, and W. E. Bolch, "Hybrid computational phantoms of the 15-year male and female adolescent: Applications to CT organ dosimetry for patients of variable morphometry," *Med. Phys.*, vol. 35, no. 6, pp. 2366–2382, 2008.

[9] P. B. Johnson *et al.*, "Hybrid patient-dependent phantoms covering statistical distributions of body morphometry in the U.S. adult and pediatric population," *Proc. IEEE*, vol. 97, no. 12, pp. 2060–2075, Dec. 2009.

[10] Y. Na, J. Zhang, X. Xu, B. Han, and P. F. Caracappa, "WE-E-BRD-08: Next-generation deformable patient modeling for Monte Carlo assessment of organ doses," *Med. Phys.*, vol. 36, no. 6, p. 2783, 2009.

[11] D. Broggio *et al.*, "Construction of an extended library of adult male 3D models: Rationale and results," *Phys. Med. Biol.*, vol. 56, no. 23, pp. 7659–7692, 2011.

[12] G. L. de la Grandmaison, I. Clairand, and M. Durigon, "Organ weight in 684 adult autopsies: New tables for a caucasoid population," *Forensic Sci. Int.*, vol. 119, no. 2, pp. 149–154, Jun. 2001.

[13] I. Clairand *et al.*, "Improvement of internal dose calculations using mathematical models of different adult heights," *Phys. Med. Biol.*, vol. 45, no. 10, pp. 2771–2785, Oct. 2000.

[14] V. F. Cassola, V. J. D. M. Lima, R. Kramer, and H. J. Khoury, "FASH and MASH: Female and male adult human phantoms based on polygon mesh surfaces: I. Development of the anatomy," *Phys. Med. Biol.*, vol. 55, no. 1, pp. 133–162, 2010.

[15] V. F. Cassola, F. M. Milian, R. Kramer, C. A. de Oliveira Lira, and H. J. Khoury, "Standing adult human phantoms based on 10th, 50th and 90th mass and height percentiles of male and female Caucasian populations," *Phys. Med. Biol.*, vol. 56, no. 13, pp. 3749–3772, 2011.

[16] W. P. Segars *et al.*, "Population of anatomically variable 4D XCAT adult phantoms for imaging research and optimization," *Med. Phys.*, vol. 40, no. 4, 2013, Art. no. 043701.

[17] W. P. Segars, G. Sturgeon, S. Mendonca, J. Grimes, and B. M. Tsui, "4D XCAT phantom for multimodality imaging research," *Med. Phys.*, vol. 37, no. 9, pp. 4902–4915, 2010.

[18] Y. Chen, R. Qiu, C. Li, Z. Wu, and J. Li, "Construction of Chinese adult male phantom library and its application in the virtual calibration of in vivo measurement," *Phys. Med. Biol.*, vol. 61, no. 5, pp. 2124–2144, 2016.

[19] A. M. Geyer, S. O'Reilly, C. Lee, D. J. Long, and W. E. Bolch, "The UF/NCI family of hybrid computational phantoms representing the current U.S. population of male and female children, adolescents, and adults—Application to CT dosimetry," *Phys. Med. Biol.*, vol. 59, no. 18, pp. 5225–5242, 2014.

[20] Y. S. Yeom, J. H. Jeong, M. C. Han, and C. H. Kim, "Tetrahedral-mesh-based computational human phantom for fast Monte Carlo dose calculations," *Phys. Med. Biol.*, vol. 59, no. 12, pp. 3173–3185, 2014.

[21] H. G. Menzel, C. Clement, and P. DeLuca, "ICRP publication 110. Realistic reference phantoms: An ICRP/ICRU joint effort. A report of adult reference computational phantoms," *Ann. ICRP*, vol. 39, no. 2, pp. 1–164, 2009.

[22] C. Fryar, Q. Gu, C. Ogden, and K. Flegal, "*Anthropometric Reference Data for Children and Adults: United States, 2011–2014* (Vital and Health Statistics), vol. 3. Hyattsville, MD, USA: Nat. Center Health Stat., 2016.

[23] M. Zankl *et al.*, "Computational phantoms of the ICRP reference male and reference female," in *Proc. 12th Congr. Int. Radiat. Protect. Assoc.*, 2008, pp. 1–9.

[24] C. L. Ogden, M. D. Carroll, C. D. Fryar, and K. M. Flegal, "Prevalence of obesity among adults and youth: United States, 2011–2014," *NCHS Data Brief*, no. 219, pp. 1–8, 2015.

[25] S. Meeuwsen, G. W. Horgan, and M. Elia, "The relationship between BMI and percent body fat, measured by bioelectrical impedance, in a large adult sample is curvilinear and influenced by age and sex," *Clin. Nutrition*, vol. 29, no. 5, pp. 560–566, Oct. 2010.

[26] Y. Schutz, U. U. Kyle, and C. Pichard, "Fat-free mass index and fat mass index percentiles in Caucasians aged 18–98 y," *Int. J. Obesity Related Metabolic Disorders*, vol. 26, no. 7, pp. 953–960, 2002.

[27] S. B. Heymsfield, M. Heo, D. Thomas, and A. Pietrobelli, "Scaling of body composition to height: Relevance to height-normalized indexes," *Amer. J. Clin. Nutrition*, vol. 93, no. 4, pp. 736–740, 2011.

[28] *National Health and Nutrition Examination Survey*, Centers for Disease Control and Prevention and National Center for Health Statistics, Hyattsville, MD, USA, 2003. [Online]. Available: http://www.cdc.gov/nchs/nhanes.htm

[29] S. R. Bozeman *et al.*, "Predicting waist circumference from body mass index," *BMC Med. Res. Methodol.*, vol. 12, p. 115, Aug. 2012.

[30] R. Mandal, A. G. Loeffler, S. Salamat, and M. K. Fritsch, "Organ weight changes associated with body mass index determined from a medical autopsy population," *Amer. J. Forensic Med. Pathol.*, vol. 33, no. 4, pp. 382–389, 2012.

[31] A. Sheikhazadi *et al.*, "Study of the normal internal organ weights in Tehran's population," *J. Forensic Legal Med.*, vol. 17, no. 2, pp. 78–83, 2010.

[32] D. K. Molina and V. J. DiMaio, "Normal organ weights in women: Part II—The brain, lungs, liver, spleen, and kidneys," *Amer. J. Forensic Med. Pathol.*, vol. 36, no. 3, pp. 182–187, 2015.

[33] D. K. Molina and V. J. DiMaio, "Normal organ weights in men: Part II—The brain, lungs, liver, spleen, and kidneys," *Amer J. Forensic Med. Pathol.*, vol. 33, no. 4, pp. 368–372, 2012.
[34] D. K. Molina and V. J. DiMaio, "Normal organ weights in women: Part I—The heart," *Amer. J. Forensic Med. Pathol.*, vol. 36, no. 3, pp. 176–181, 2015.
[35] D. K. Molina and V. J. DiMaio, "Normal organ weights in men: Part I—The heart," *Amer. J. Forensic Med. Pathol.*, vol. 33, no. 4, pp. 362–367, 2012.
[36] Q. He *et al.*, "Smaller organ mass with greater age, except for heart," *J. Appl. Physiol. (1985)*, vol. 106, no. 6, pp. 1780–1784, 2009.
[37] S. B. Heymsfield, D. Gallagher, L. Mayer, J. Beetsch, and A. Pietrobelli, "Scaling of human body composition to stature: New insights into body mass index," *Amer. J. Clin. Nutrition*, vol. 86, no. 1, pp. 82–91, 2007.
[38] H. A. Perven, A. S. Nurunnabi, S. Ara, and M. U. Jahan, "Cadaver study of the volume of the ovary in Bangladeshi women," *Bangladesh Med. Res. Council Bull.*, vol. 40, no. 1, pp. 15–17, 2014.
[39] T. W. Kelsey *et al.*, "A validated normative model for human uterine volume from birth to age 40 years," *PLoS ONE*, vol. 11, no. 6, 2016, Art. no. e0157375.
[40] S.-J. Zhang *et al.*, "Relationship between age and prostate size," *Asian J. Androl.*, vol. 15, no. 1, pp. 116–120, 2013.
[41] S. J. Xia, X. X. Xu, J. B. Teng, C. X. Xu, and X. D. Tang, "Characteristic pattern of human prostatic growth with age," *Asian J. Androl.*, vol. 4, no. 4, pp. 269–271, 2002.
[42] A. Chouker *et al.*, "Estimation of liver size for liver transplantation: The impact of age and gender," *Liver Transplant.*, vol. 10, no. 5, pp. 678–685, 2004.
[43] T. W. Kelsey *et al.*, "Ovarian volume throughout life: A validated normative model," *PLoS ONE*, vol. 8, no. 9, 2013, Art. no. e71465.
[44] ICRP, "Radiation dose to patients from radiopharmaceuticals. Addendum 3 to ICRP publication 53. ICRP publication 106," *Ann. ICRP*, vol. 38, nos. 1–2, pp. 1–197, 2008.
[45] T. Xie, W. E. Bolch, C. Lee, and H. Zaidi, "Pediatric radiation dosimetry for positron-emitting radionuclides using anthropomorphic phantoms," *Med. Phys.*, vol. 40, no. 10, 2013, Art. no. 102502.
[46] T. Xie, N. Kuster, and H. Zaidi, "Effects of body habitus on internal radiation dose calculations using the 5-year-old anthropomorphic male models," *Phys. Med. Biol.*, vol. 62, no. 15, pp. 6185–6206, 2017.
[47] W. E. Bolch, K. F. Eckerman, G. Sgouros, and S. R. Thomas, "MIRD pamphlet no. 21: A generalized schema for radiopharmaceutical dosimetry—Standardization of nomenclature," *J. Nucl. Med.*, vol. 50, no. 3, pp. 477–484, 2009.
[48] Bayer HealthCare. (2017). *Radimetrics Enterprise Platform: Dose Management Solution*. [Online]. Available: http://www.radiologysolutions.bayer.com/products/ct/dosemanagement/rep/
[49] M. Cristy and K. Eckerman, "Specific absorbed fractions of energy at various ages from internal photon sources. I methods, II one year old, III five year old, IV ten year old, V fifteen year old male and adult female, VI new-born and VII adult male," Oak Ridge Nat. Lab., Oak Ridge, TN, USA, Rep. ORNL/TM 8381/V1-V7, 1987.
[50] A. Akbarzadeh, M. R. Ay, H. Ghadiri, S. Sarkar, and H. Zaidi, "Measurement of scattered radiation in a volumetric 64-slice CT scanner using three experimental techniques," *Phys. Med. Biol.*, vol. 55, no. 8, pp. 2269–2280, 2010.
[51] T. Xie, P.-A. Poletti, A. Platon, C. D. Becker, and H. Zaidi, "Assessment of CT dose to the fetus and pregnant female patient using patient-specific computational models," *Eur. Radiol.*, vol. 28, no. 3, pp. 1054–1065, 2018.
[52] W. H. Sheldon, S. S. Stevens, and W. B. Tucker, *The Varieties of Human Physique: An Introduction to Constitutional Psychology*. New York, NY, USA: Harper, 1940.
[53] D. P. Kingma and M. Welling, "Auto-encoding variational bayes," in *Proc. Int. Conf. Learn. Represent. (ICLR)*, Banff, AB, Canada, 2014, pp. 1–14.
[54] I. Goodfellow *et al.*, "Generative adversarial networks," in *Proc. Neural Inf. Process. Syst. (NIPS)*, Montreal, QC, Canada, 2014, pp. 1–9.
[55] T. Neff, C. Payer, D. Stern, and M. Urschler, "Generative adversarial network based synthesis for supervised medical image segmentation," in *Proc. OAGM ARW Joint Workshop*, Vienna, Austria, 2017, pp. 140–145.